Supporting Online Material for

When Fear Is Near: Threat Imminence Elicits Prefrontal–Periaqueductal Gray Shifts in Humans

Dean Mobbs,* Predrag Petrovic, Jennifer L. Marchant, Demis Hassabis, Nikolaus Weiskopf, Ben Seymour, Raymond J. Dolan, Christopher D. Frith

*To whom correspondence should be addressed. E-mail: d.mobbs@fil.ion.ucl.ac.uk

Published 24 August 2007, *Science* **317**, 1079 (2007)
DOI: 10.1126/science.1144298

This PDF file includes:

Methods and Materials

Subjects

We scanned 19 healthy subjects. All were English speaking, right-handed, had normal or corrected vision and were screened for a history of psychiatric or neurological problems. All subjects gave informed consent and the study was approved by the joint Ethics committee of the National Hospital for Neurology and Neurosurgery (UCLH NHS Trust) and the Institute of Neurology. One subject was discarded from the analysis due to poor behavioural performance during scanning; three subjects were not analyzed due to technical problems with the scanner and one was discarded for being left-handed leaving a total of 14 subjects (mean age and s.d. 25.9 ± 3.9).

Experimental Procedures

Pain Calibration. A cutaneous electrical pain stimulation was applied to the dorsum of the right hand. Each subject was allowed to calibrate the shocks to their own comfort level. The intensity of the shock was tested before the experiment and set to the maximum tolerable painful stimulation (below 20mA).

AI Program. A recursive breadth-first flood-fill search algorithm (1) was implemented to control the behavior of the artificially intelligent (AI) predator ($AI_{predator}$). All valid adjacent positions (i.e. not wall blocks) from the current position (maximum 4) were considered for the next movement, with the distance to the target computed for each. Then the valid adjacent position with the shortest distance to the prey was chosen as its next movement. For mazes with no dead ends, as used in this study, this is the optimal strategy for the $AI_{predator}$. To dissociate spatial and temporal elements of imminence, and also allow for more variation in distance for the parametric analyses, a small jitter was introduced to the speed of the $AI_{predator}$ which randomly changed every 4 seconds from the starting speed (see speed calibration).

Speed Calibration. The $AI_{Predator}$ was programmed to be slightly faster than the subject's calibrated speed. The speed was dependent on the one chosen during the subjects' speed calibration trials and was

typically in the range of 10% faster or slower. Subjects used a key-pad to navigate the blue triangle and were given time to practice the task in and out of the scanner. To reduce any motion and confounds due to repetitive key pressing, the blue triangle could be moved by continuously holding the keys. After each practice session, subjects' behavioral data was viewed to see how often they escaped the $AI_{Predator.}$ Subjects were only scanned after they could fully control the navigation of the blue triangle and could escape the $AI_{Predator}$ more than 25% of the time.

Paradigm. Subjects were presented with a 2D maze containing a 9 x 13 rectangle grid of walls (black squares) and paths (white squares). Based on ecological models of predator and prey interactions, the paradigm consisted of three phases. All experimental conditions commenced with a *Neutral phase* where a pre-programmed artificially intelligent (AI) gray circle ($AI_{Neutral}$) appeared at the left-bottom side of the maze. The $AI_{Neutral}$ was presented on average for 6 s (jitter ± 2 s) and programmed to wander the maze indiscriminately. Following this, the *Cue phase* commenced with the $AI_{Neutral}$ changing into a predator AI ($AI_{Predator}$) or a yoked control condition. The change from $AI_{Neutral}$ to $AI_{Predator}$ was signaled by the circle flashing between red and gray. The flashing $AI_{Predator}$ appeared for 2 s and during this time it wandered the maze indiscriminately. Directly following this, subjects where also informed for 2 s of the amount of cutaneous electrical shock they would receive if the $AI_{Predator}$ captured them – for example one shock ($AI_{Predator}^{Low}$) or three shocks ($AI_{Predator}^{High}$). The switch to the blue circle indicated to the subject that they would view the control condition with no consequences During the *Cue phase,* subjects were unable to move the blue triangle situated in the top right-hand corner of the maze. The *Chase phase* began with the $AI_{Predator}$ ceasing to flash and the subject moving the blue triangle to escape the $AI_{Predator}$ or to mimic the movements of the triangle in a replay of a previous experimental condition (yoked control condition). There were two additional conditions in which participants chased an AI prey through the maze.

To ensure that subjects would not anticipate the end of the chase, we randomly varied the duration of each $AI_{Predator}$ encounter (e.g. 16, 20, 24, 28, 32s). The subjects were not informed that the length of trials varied or given any indication of how much time they had on each trial. To enhance the

feelings of spatial distance, mazes were intentionally designed so that chases were long unimpeded runs with no dead-ends. Each block was interleaved with 8, 10, or 12 s black screen. The task took approximately 60 mins and included 30 trials of $AI_{Predator}^{High}$. Two additional conditions were presented – first, we wished to see if there were any pain magnitude effects. We therefore presented each subject with 12 trials of $AI_{Predator}^{Low}$. As a control condition, subjects viewed play back of a previous trial and were asked to mimic the movements of the triangle, thus controlling the sensorimotor aspects of the task (12 trials). Each trial was interleaved with 8, 10, or 12 s of a black screen. See Fig S1 for more details on timing. There was an additional condition in which subjects were required to chase and capture prey. The results of this condition will be described elsewhere

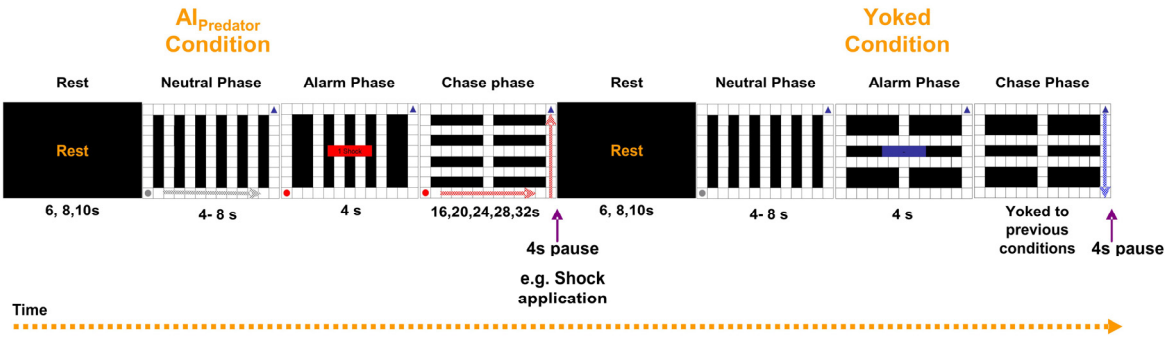

Fig S1. Illustration of the paradigm timing. Participants were presented with 84 randomly allocated experimental trial. Each trial includes the three conditions of Neutral, Cue and Chase phases. Each trial began with a blank rest screen for average of 8s. This was followed by the *Neutral Phase* which was presented for an average of 6s. Directly following this, the subject was presented with the *Cue Phase*, where a red or blue circle indicated the condition $AI_{Predator}$, or yoked control, respectively. This phase also indicated the magnitude of pain (1 or 3 shocks). The *Chase Phase* began once the AI stopped flashing and subject could move the blue triangle. This phase was randomly timed with the subject not knowing how long the condition would last. The shocks were administered only when there was contact with the AI. The shock was applied 2s after contact.

Behavioral recordings. We recorded the amount of time the subject was in the maze for each

experimental condition. We also recorded the percentage of times the subject was caught by the $AI_{Predator}$ at both magnitude levels.

Post-Scan Questionnaire. After scanning, subjects completed a post-scan questionnaire which asked them to indicate on a 10-point analog Likert scale how much they dreaded being chased by the $AI_{Predator}$ and how confident they were of escape.

fMRI acquisition. A 3T Allegra head scanner with standard transmit-receive head coil was used to acquire functional data with a single-shot gradient echo isotropic high-resolution echo-planar imaging (EPI) sequence (matrix size: 128x128; Fov: 192x192 mm^2; in-plane resolution: 1.5x1.5 mm^2; 50 slices with interleaved acquisition; slice thickness: 1.5 mm with no gap between slices; TE: 30 ms; assymetric echo shifted forward by 26 phase-encoding (PE) lines; acquisition time per slice: 102 ms; TR: 5100 ms; echo spacing: 560 μs; receiver bandwidth: 250 kHz; 30% ramp sampling; 2-fold read oversampling to allow for k-space regridding; z-shim gradient compensation prepulse: -1.4 mT/m*ms; read gradient amplitude 34.47mT/m; read gradient slew rate: 344.7 mT/m/ms; (2)). In order to maximise statistical power we used only 50 slices that were optimised to cover brainstem and angled at -30° to cover the ventral ACC and mObfc. The slice tilt, z-shim and high spatial resolution further reduced susceptibility-related signal loss in the mObfc (3, 4). In addition, field maps using a double echo FLASH sequence were recorded for correction of susceptibility-related geometric distortions in the EPI images (5). A high-resolution T1-weighted structural scan was obtained for each subject (1 mm isotropic resolution 3D MDEFT, (6)) and coregistered to the subject's mean EPI image. The mean of all individual structural images permitted the anatomical localization of the functional activations at the group level.

fMRI analysis. Statistical parametric mapping (SPM2; Wellcome Trust Centre for Neuroimaging, www.fil.ion.ucl.ac.uk/spm) was used to preprocess all fMRI data and included spatial realignment, normalization and smoothing. To control for motion, all functional volumes were realigned to the mean volume. Using the FieldMap toolbox, field maps were estimated from the phase difference between the

images acquired at the short and long TE and unwrapped (5). Voxel displacements in the EPI image were determined from the field map and EPI imaging parameters. Distortions were corrected by applying the inverse displacement to the EPI images. Images were spatially normalized (7) to standard space Montreal Neurological Institute (MNI) template (8) with a resample voxel size of 1 x 1 x 1 mm and smoothed using a Gaussian kernal with an isotropic full width at half maximum (FWHM) of 4 mm. In addition, high-pass temporal filtering with a cut-off of 128 s was applied to remove low-frequency drifts in signal and global changes were removed by proportional scaling. Following preprocessing, statistical analysis was conducted using the general linear model.

Analysis was performed to determine each subject's voxel-wise activation during $AI_{Predator}$ and yoked conditions. Event-related neural activity was modeled with delta functions representing block onsets convolved with the canonical hemodynamic response function and time derivative to provide a regressor for event-related BOLD-signal changes. Movement regressors where also placed in the matrix. Random effects analysis (9) was used for group statistics. A statistical threshold of $P < 0.05$ corrected for multiple spatial comparisons across the whole-brain was used, except for a priori hypothesized regions which were thresholded at $P < 0.001$ uncorrected (only clusters involving $k>30$ or more contiguous voxels are reported). These a priori regions of interest included the periaqueductal gray, amygdala, medial orbital frontal cortex, dorsal raphe nucleus, ventrolateral prefrontal cortex, ventromedial prefrontal cortex, insula and rostral anterior cingulate cortex.

Supplementary Results

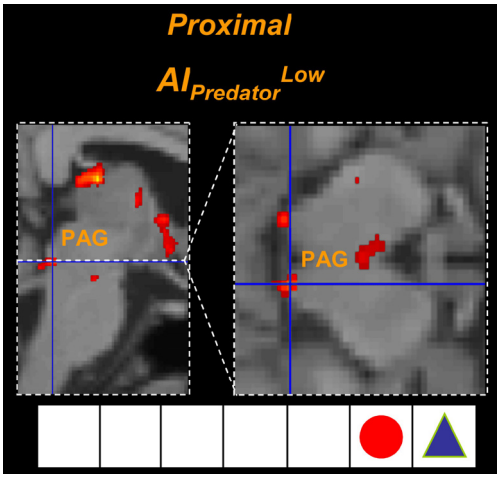

Fig S2. fMRI results illustrating the imminence driven PAG activity in the $AI_{\_Predator}^{Low}$ condition. Increased activity in right PAG (6, -33, -14; Z=3.02) for the proximal $AI_{\_Predator}^{Low}$.

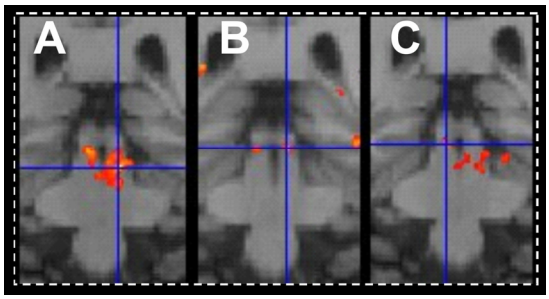

Fig S3. Coronal view of fMRI results illustrating the imminence driven PAG activity in the (A) $AI_{\_Predator}^{high}$, (B) $AI_{\_Predator}^{low}$, and (C) $AI_{\_Predator}^{high}$ minus $AI_{\_Predator}^{low}$ contrasts.

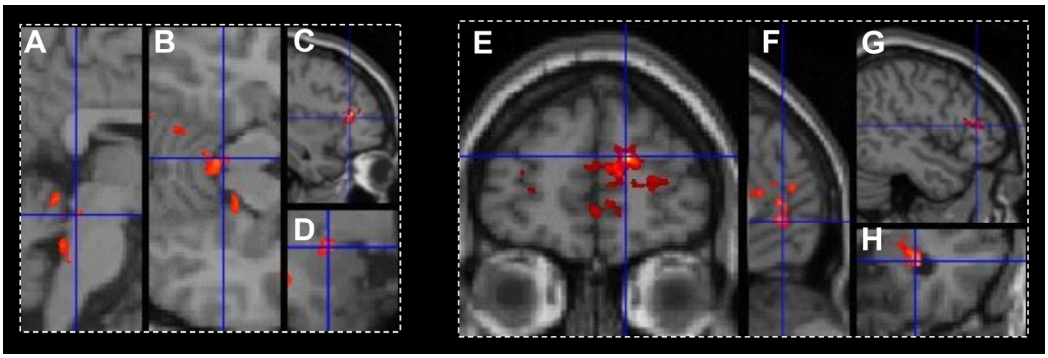

Fig S4. Direct comparison between high and low AI_predators.

For the high minus the low predator we found increased PAG activity shown on (A) sagittal and (B) axial slices (MNI: -3, -32, -15; Z=3.33); (C) sagittal slice illustrating the increased dlPFC activity (37, 33, 9; Z=4.28**), and (D) increased dorsal amygdala activity (-23, 0, -15; Z=3.06). For the opposite contrast, low minus the high predator resulted in increased (E) dorsal medial prefrontal activity (15, 54, 20; Z=4.86**), (F) vmPFC activity (-1 51, -1, 3.81), dlPFC (-35 39 8; Z=5.15**) and ventral amygdala activity (31, -4, -23; Z=4.09). All are results are at P<0.001 uncorrected except for those flagged which are P<0.05 corrected for multiple comparisons**.

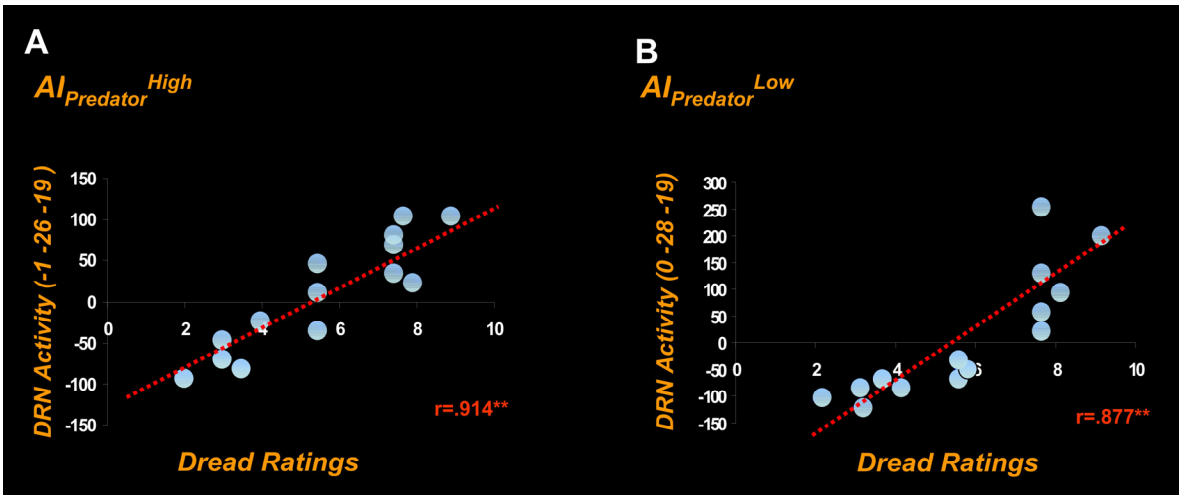

Fig S5 Individual differences in dread ratings and dorsal raphe nuclei (DRN) activity.

Dread of interaction with the $AI_{Predator}$. Correlated with increased DRN acivity for the (A) $AI_{Predator}^{High}$ and (B) $AI_{Predator}^{Low}$ conditions.

Supplementary Tables

Table S1. Coordinates in MNI space and associated z-scores showing the BOLD differences cues to $AI_{Predator}$ Cue relative to yoked context

Brain Regions	**Z scores**	**Coordinates**		
		X	**Y**	**Z**
***$AI_{Predator}$* Cue**				
R ventral ACC	4.56	13	32	-14
L rACC	3.85	-6	41	22
L dorsal rACC	4.23	-8	18	30
L vlPFC	4.01	-29	48	-6
L vmPFC	3.48	-4	39	-13
R mObfc	3.42	6	49	-19
R mPFC	3.67	3	54	-4
Premotor**	4.23	40	20	28

All values P<0.001 uncorrected. ** P<0.05 corrected for multiple comparisons.

Table S2. Coordinates in MNI space and associated z-scores showing the BOLD differences cues to $AI_{Predator}$ block relative to yoked context

Brain Regions	**Z scores**	**Coordinates**		
		X	**Y**	**Z**
$AI_{Predator}$ – Yoked block				
R PAG**	4.87	3	-25	-7
L PAG**	4.94	-2	-28	-8
L Cerebellum**	5.48	-5	-63	-13
R Pulvinar**	4.63	3	-22	11
L Caudate**	5.09	-17	2	25
R Caudate**	4.85	16	-13	20
Yoked - $AI_{Predator}$ block				
L Medial PFC**	5.50	-5	48	17
R vmPFC**	4.63	3	37	-9
R amygdala**	4.94	22	-2	-18
R ventral amygdala**	4.70	28	-6	-27

All values P<0.001 uncorrected. ** P<0.05 corrected for multiple comparisons.

Table S3. Coordinates in MNI space and associated z-scores showing the BOLD differences for parametric regressors associated with distal and proximal distance for the $AI_{Predator}$ conditions

Brain Regions	**Z scores**	**Coordinates**		
		X	**Y**	**Z**
$AI_{Predator}^{High\ distal}$				
L mObfc	3.66	-8	35	-13
L mObfc	3.36	-5	27	-14
R BLA	3.77	32	-4	-24
R dorsal striatum**	4.62	16	16	2
R Lateral PFC	3.32	45	34	-8
$AI_{Predator}^{Low\ distal}$				
L mObfc	3.93	-10	38	-11
L BLA	3.51	-31	-2	-25
R ACC	3.20	2	42	6
$AI_{Predator}^{High\ proximal}$				
L periaqueductal gray	3.58	-3	-33	-15
R periaqueductal gray	3.73	8	-32	-21
R CeA	4.78	32	4	-13
R premotor	4.52	60	18	8
R pons	3.57	2	-27	-28
R dACC	4.14	7	20	30
$AI_{Predator}^{Low\ proximal}$				
R periaqueductal gray	3.02	6	-33	-14
R dACC	3.40	5	28	17
R vmPFC	4.37	8	59	-1
L caudate**	4.43	-10	16	13
R caudate**	3.85	20	7	10
R dlPFC**	3.85	30	47	27
$AI_{Predator}^{High} - AI_{Predator}^{Low}$				
R dlPFC**	4.28	37	33	9
R hippocampus	3.52	38	-13	-17
L periaqueductal gray	3.33	-3	-32	-15
L CeA	3.06	-23	0	-15
$AI_{Predator}^{Low} - AI_{Predator}^{High}$				
L vmPFC	3.81	-1	51	-1
R dmPFC**	4.86	15	54	20
L dlPFC**	5.15	-35	39	8
R BLA	4.09	31	-4	-23
L fusiform gyrus	4.01	-32	-73	-14

All values P<0.001 uncorrected . ** P<0.05 corrected for multiple comparisons.

Table S4. Coordinates in MNI space and associated z-scores showing the BOLD differences for parametric regressors associated with distance and dread ratings

Brain Regions	**Z scores**	**Coordinates**		
		X	**Y**	**Z**
AI_{Prey}^{High} **increased dread**				
L DRN	4.65	-1	-26	-19
R SN	3.90	7	-20	-15
R Medial PFC**	3.90	18	58	7
R ACC	3.62	5	42	15
R mObfc	3.42	5	42	-13
R dlPFC	4.09	49	38	11
R PAG	3.14	11	-32	-18
AI_{Prey}^{Low} **increased dread**				
L Medial PFC	3.89	-3	61	12
DRN	4.29	0	-28	-19
L PAG	3.33	-5	-32	-18
L Pons	3.90	-9	-32	-32
L vlPFC**	4.43	-36	45	-2
L Cerebellum	4.73	-3	-61	-32
R Cerebellum	4.47	29	-57	-28
AI_{Prey}^{High} **– decreased dread**				
dACC	4.25	0	17	26
putamen	3.41	24	11	1
L fusiform	3.79	-45	-66	-8
L ventral striatum	3.74	-20	10	-11
R posterior Hippocampus	3.67	34	-40	-6
L insula	3.64	-31	24	-4
R mObfc	3.37	3	38	-17
AI_{Prey}^{Low} **- decreased dread**				
Dorsal striatum	5.00	23	-2	16
R middle temporal gyrus	3.95	57	-24	-11
R lateral occipital lobe	3.92	42	-76	-13
L dlPFC	3.86	-39	34	15
R vlPFC	3.81	35	49	-1
L subgenul	4.34	-4	29	-8
MPFC	3.56	-3	48	24
Superior colliculus	3.60	-3	-33	-5

All values P<0.001 uncorrected . ** P<0.05 corrected for multiple comparisons.

Table S5. Coordinates in MNI space and associated z-scores showing the BOLD differences for parametric regressors associated with distance and confidence of escape ratings

Brain Regions	**Z scores**	**Coordinates**		
		X	**Y**	**Z**
AI_{Prey}^{High} **increased confidence of escape**				
R CeA	4.05	27	7	-16
R Ventral Amygdala	3.10	19	-7	-24
L NAcc	3.62	-11	16	-7
R Ventral PFC	3.48	17	47	-4
L Dorsal PFC	3.66	-5	44	30
R Anterior insula**	5.06	34	22	-10
AI_{Prey}^{High} **decreased confidence of escape**				
R PAG	3.19	2	-29	-19
R Dorsal rACC	3.07	6	24	28
R MFD	3.21	7	54	28
R Pulvinar	3.36	6	-26	10
L Thalamus	4.13	-8	-19	4
R Insula	3.42	49	-7	7
AI_{Prey}^{low} **increased confidence of escape**				
L OFC	4.05	-2	34	-20
R Anterior amygdala	3.68	28	9	-25
R vmPFC	4.36	12	51	-8
AI_{Prey}^{low} **decreased confidence of escape**				
L PAG***	2.63	-3	-37	-20
R MFD	4.44	7	41	31

All values P<0.001 uncorrected. ** P<0.05 corrected for multiple comparisons. *** P<0.005 uncorrected

References

1. S. J. Russell, & Norvig, P., *Artificial Intelligence: A Modern Approach.* (Pearson Education, Inc, ed. 2nd edition, 2003).

2. J. D. Haynes, Deichmann, R., Rees, G. . *Nature* **438**, 496-499 (2005).

3. N. Weiskopf, Hutton, C., Josephs, O., Deichmann, R., *NeuroImage* **2**, 493-504 (2006).

4. N. Weiskopf, Hutton, C., Josephs, O., Turner, R., Deichmann, R., *Magnetic Resonance Materials in Physics, Biology and Medicine* **20**, 39-49 (2007).

5. C. Hutton, Bork, A., Josephs, O., Deichmann, R., Ashburner, J., Turner, R., *NeuroImage* **16**, 217-240 (2002).

6. R. Deichmann, Schwarzbauer,C., Turner,R., *NeuroImage* **21**, 757-767 (2004).

7. J. Ashburner, Friston, K.J., *Human Brain Mapping* **7**, 254-66 (1999).

8. J. C. Mazziotta, Toga, A.W., Evans, A., Fox, P., Lancaster, J., in *The International Consortium for Brain Mapping (ICBM)*. (1995), vol. 21.

9. W. H. Penny, Friston, K., in *Human Brian Function* R. S. J. Frackowiak, Ed. (Academic Press, London, 2003).